APL Electronic Devices

RESEARCH ARTICLE | DECEMBER 10 2025

Reduced thermal resistance of Al-rich AlGaN HEMTs via top-side diamond integration

James Spencer Lundh ✉ ; Brianna A. Klein ; Tatyana I. Feygelson; Daniel J. Pennachio ; Andrew A. Allerman; GlenAsia Gonzalez; Emma G. Rocco ; Hannah N. Masten ; Geoffrey M. Foster; Katie R. Gann ; Alan G. Jacobs ; Andrew M. Armstrong ; Ethan A. Scott ; Patrick E. Hopkins; Marko J. Tadjer ; Bradford B. Pate ; Karl D. Hobart ; Michael A. Mastro

APL Electronic Devices 1, 046126 (2025)
https://doi.org/10.1063/5.0304018

APL Electronic Devices ARTICLE pubs.aip.org/aip/aed

Reduced thermal resistance of Al-rich AlGaN HEMTs via top-side diamond integration

Cite as: APL Electron. Devices 1, 046126 (2025); doi: 10.1063/5.0304018
Submitted: 25 September 2025 • Accepted: 19 November 2025 •
Published Online: 10 December 2025

James Spencer Lundh,[1,a)] Brianna A. Klein,[2] Tatyana I. Feygelson,[1] Daniel J. Pennachio,[1] Andrew A. Allerman,[2] GlenAsia Gonzalez,[2] Emma G. Rocco,[1] Hannah N. Masten,[3] Geoffrey M. Foster,[3] Katie R. Gann,[4] Alan G. Jacobs,[1] Andrew M. Armstrong,[2] Ethan A. Scott,[5] Patrick E. Hopkins,[5] Marko J. Tadjer,[1] Bradford B. Pate,[1] Karl D. Hobart,[1] and Michael A. Mastro[1]

AFFILIATIONS

[1] U.S. Naval Research Laboratory, Washington, District of Columbia 20375, USA
[2] Sandia National Laboratories, Albuquerque, New Mexico 87123, USA
[3] Amentum Services, Inc., Residing at U.S. Naval Research Laboratory, Washington, District of Columbia 20375, USA
[4] National Research Council Postdoctoral Fellow, Residing at U.S. Naval Research Laboratory, Washington, District of Columbia 20375, USA
[5] Department of Mechanical and Aerospace Engineering, University of Virginia, Charlottesville, Virginia 22904, USA

[a)] **Author to whom correspondence should be addressed:** james.s.lundh.civ@us.navy.mil

ABSTRACT

We report back-end-of-line growth of nanocrystalline diamond (NCD) on ultrawide bandgap (UWBG) high Al content aluminum gallium nitride (AlGaN) channel high electron mobility transistors for thermal management. A thin (~15 nm) silicon nitride (SiN_x) interlayer was deposited to protect the device surface before performing a low temperature (500 °C) NCD growth process in an attempt to protect the gates on these fully fabricated devices. Notably, atomic force microscopy showed that the maximum lateral grain size exceeded 300 nm even though the film thickness was ~250 nm. Comparing electrical (DC) performance before and after NCD growth, the gate leakage increased by ~10^2 after NCD growth. Despite the lower NCD growth temperature, intermixing of the Ni and Au was observed in the Schottky gate metal stack; however, we believe there is another mechanism, possibly hydrogen-related, that is responsible for the measured increase in gate leakage. Regarding thermal management, the device-level thermal resistance (quantified using the average gate temperature rise measured by thermoreflectance imaging) was reduced by 29% through the incorporation of the top-side diamond film. Using time-domain thermoreflectance, the thermal conductivity of the ≈250 nm thick NCD film was measured to be 45 ± 25 W m^{-1} K^{-1}. This is expected to be at least 5× greater than the thermal conductivity of the thin disordered AlGaN alloy. There could also be a coupled electrothermal component contributing to the reduced temperature rise from electric field spreading and consequent heat spreading. This study demonstrates a promising first step toward device-level thermal management of high power UWBG Al-rich AlGaN devices.

INTRODUCTION

Ultrawide bandgap (UWBG) semiconductors, such as $Al_xGa_{1-x}N$, AlN, β-Ga_2O_3, BN, GeO_2, and diamond, are receiving significant interest and investment in the device research community to realize the next generation of radio frequency (RF) and power electronics.[1,2] UWBG semiconductor device technologies offer the potential for increased radiation tolerance, higher temperature operation, higher voltage blocking capabilities, and higher power output. $Al_xGa_{1-x}N$-based semiconductor devices are an enticing option that benefits from the natural transition of the research, development, and infrastructure of GaN crystal growth, processing, and device fabrication. For lateral devices, this includes transitioning from GaN channel high electron mobility transistors (HEMTs) to $Al_xGa_{1-x}N$ channel HEMTs,[3,4] for which the development of low contact resistance Ohmic contacts has been

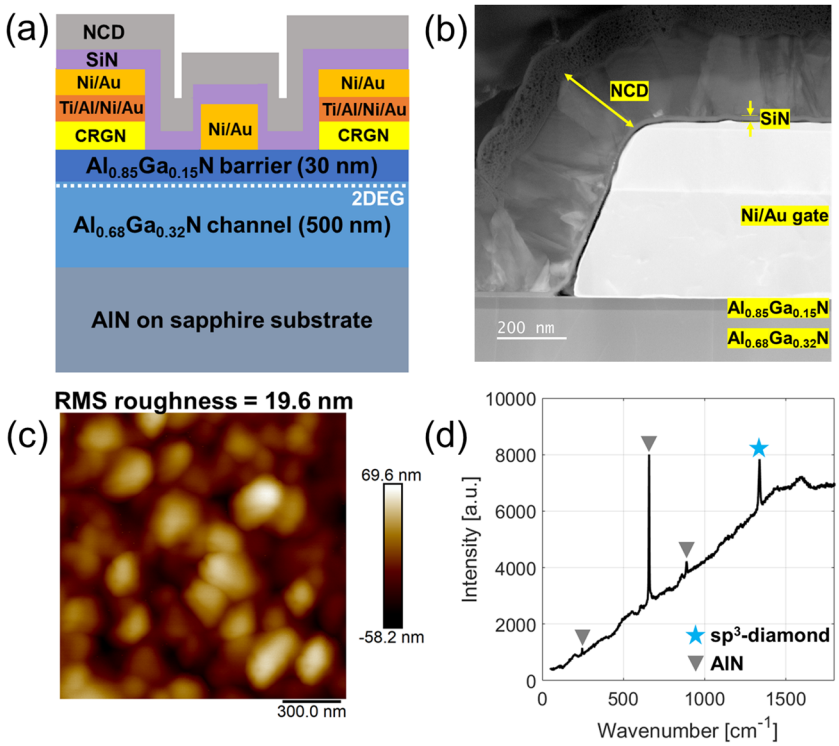

FIG. 1. (a) Cross-sectional schematic of the AlGaN channel HEMT. (b) Cross-sectional MAADF image of the HEMT with diamond. (c) AFM and (d) Raman of the diamond film.

a significant hurdle until recent demonstrations of reverse-graded nitride regrown contacts.[5–7]

With shrinking device footprints and increasing power demands, an inevitable barrier to widespread adoption and reliability is device self-heating. Overcoming this thermal challenge for GaN-based devices has been extensively studied for years, and this research is ongoing.[8] This is expected to become even more challenging for $Al_xGa_{1-x}N$ due to its lower thermal conductivity, resulting from disordered alloy scattering.[9,10] As such, it is imperative to consider and incorporate thermal management solutions during the earlier stages of device design and development. For GaN HEMTs, top-side diamond integration has been shown to be an effective method for near-junction thermal management.[11] Accordingly, in this study, we demonstrate back-end-of-line (BEOL) low temperature (500 °C) nanocrystalline diamond (NCD) growth on high Al-content $Al_xGa_{1-x}N$ (x = 0.68) channel HEMTs for top-side thermal management [Fig. 1(a)].

EXPERIMENTAL METHODS

Metal-organic chemical vapor deposition (MOCVD) was used to grow the HEMT epitaxial layers on AlN/sapphire templates [Fig. 1(a)]. These include a 3.4 μm thick AlN buffer, a 500 nm thick unintentionally doped (UID) $Al_{0.68}Ga_{0.32}N$ channel, and a 30 nm thick $Al_{0.85}Ga_{0.15}N$ barrier (Si-doped, 6×10^{18} cm^{-3}). Standard contact lithography was used to fabricate the HEMTs. An W layer was deposited, and footprints for ohmic contact regrowth were opened. Compositional reverse graded (CRGN) Ohmic regrowth[12] consisted of (i) a 10 nm thick $Al_{0.85}Ga_{0.15}N$ layer (Si-doped, 6×10^{18} cm^{-3}), (ii) a 100 nm thick n+ (Si-doped, 2–12 $\times$ 10^{19} cm^{-3}) compositionally reverse graded $Al_xGa_{1-x}N$ layer (x = 85% down to x = 14%), and (iii) a 30 nm thick $Al_{0.14}Ga_{0.86}N$ layer (Si-doped, 1.2 $\times$ 10^{20} cm^{-3}) sequentially grown using MOCVD. The access region was revealed by removing the ohmic regrowth and mask using BCl_3/Cl_2-based inductively coupled plasma etching and wet etching. Ohmic contacts were formed via e-beam evaporation of Ti/Al/Ni/Au (25/100/15/50 nm) followed by rapid thermal annealing (700 °C, 30 s, N_2). Finally, the gate metal (Ni/Au, 20/450 nm) was deposited via e-beam evaporation on both the gate regions and over the Ohmic contacts. The devices had a gate length (L_G) of 3 μm, a gate width (W_G) of 660 μm, and gate-source (L_{GS}) and gate-drain (L_{GD}) spacings of 3.5 μm. From circular transmission line method (CTLM) measurements, the specific contact resistivity (ρ_c) and sheet resistance (R_{sh}) were measured to be 6.7×10^{-4} Ω cm^2 and 6.3 kΩ/sq, respectively.

Following fabrication, a 15 nm thick plasma-enhanced CVD silicon nitride (SiN_x) layer was deposited at 300 °C as a protective interlayer for aluminum gallium nitride (AlGaN) prior to diamond growth. Subsequently, a ≈0.25 μm thick NCD cap was grown via microwave plasma CVD at 500 °C after the AlGaN surface was seeded with detonation nanodiamond particles via an ultrasonication process.[13] The total NCD growth duration was ≈9 h due to reduced growth rates at lower growth temperatures. The NCD and SiN_x interlayer were etched via O_2 and SF_6 plasma, respectively, from the metal pads for electrical probing.

Surface roughness and lateral grain size of the NCD film were measured using a Bruker atomic force microscope (AFM). Raman spectroscopy was performed to qualitatively assess the crystalline

quality of the NCD using a Thermo Scientific DXR3xi Raman spectrometer. For the Raman measurements, a 532 nm laser was used with a 100× objective and a 25 μm confocal hole. The Raman spectrum was acquired via averaging 100 scans taken with an acquisition rate of 8 Hz and a laser power of 5 mW. Because the energy of the 532 nm laser is sub-bandgap for the semiconductors in the device epitaxial layers (NCD, SiNx, AlGaN, and AlN) and the sapphire substrate, laser heating was assumed to be negligible. A Nion UltraSTEM 200X scanning transmission electron microscope (STEM) with energy dispersive x-ray spectroscopy (EDS) capability was used for cross-sectional imaging and elemental analysis of the device. DC electrical characteristics of the HEMTs were measured using a Keithley 4200A-SCS parameter analyzer.

To measure the operating temperature of the uncapped and NCD-capped AlGaN HEMTs, we elected to use thermoreflectance imaging, a method that relies on the temperature dependence of the reflectance of the device surface. The thermoreflectance system used (TMX Scientific T°Imager) is optimized for use with near-UV and visible wavelengths (365–700 nm). Therefore, we used this method to probe the Au-coated gate electrode, which has been demonstrated extensively for estimating peak temperature rise in lateral transistors.[14–23] For the device thermal measurements, we used a probing wavelength of 530 nm, a 100× objective, and a device pulse-width of 100 ms, a time-scale that has been shown to be sufficient for lateral AlGaN transistors to reach a quasi-steady state condition.[22]

The thermal conductivity of the NCD film was measured using time-domain thermoreflectance (TDTR) on a witness sample (500 μm thick Si substrate) that underwent both the SiN_x deposition and NCD growth. For sample preparation, a metal transducer (80 nm thick Al) was deposited via e-beam evaporation after a solvent clean (acetone/isopropyl alcohol). The TDTR measurements were performed in a two-tint configuration[24] using a pulsed Ti:Sapphire laser with a pulse width of 150 fs, a repetition rate of 80 MHz, a central wavelength of 808 nm, and a full width at half maximum (FWHM) of 13 nm. The laser is split into two beam paths (pump and probe) with a half-wave plate and a polarizing beam-splitting cube. The pump provides periodic heating to the sample, which is modulated at 8.4 MHz with an electro-optic modulator. The probe pulses are time-delayed relative to the pulses of the pump with a linear delay stage, which provides up to 5.5 ns of delay. The probe and pump beams are recombined with a dichroic mirror and are concentrically focused on the sample surface, which produces $1/e^2$ diameters of 12 and 18 μm, respectively. The reflected probe light is detected by a photodetector connected to a lock-in amplifier, which is synchronized to the modulation frequency. The reflected signal is recorded as a function of the delay time between the pump and probe pulses.

To extract thermal properties, we analyze the ratio of the in-phase and out-of-phase lock-in signals using a thermal model,[25] where parameters of interest are obtained via least-squares optimization. We model the sample as a four-layer stack: (1) a nominally 80 nm thick Al transducer, (2) a 260 nm thick NCD, (3) a 13.4 nm thick SiN_x interlayer, and (4) a 500 μm thick silicon substrate. The Al transducer thickness and thermal conductivity—measured from ps ultrasonic measurements[26] and four-point probe measurements on a witness sample from the Al transducer deposition—are 81 ± 3 nm and 149 ± 5 Wm^{-1} K^{-1}, respectively. Additional TDTR measurements on a Si substrate and a SiN_x-on-Si sample were performed to help determine a Si thermal conductivity (130 ± 9 W m^{-1} K^{-1}) and an effective SiN_x thermal conductivity (0.73 ± 0.09 W m^{-1} K^{-1}). In this model, the thermal interface resistances are lumped into an effective thermal conductivity of the SiN_x interlayer in order to reduce the number of fitting parameters. The volumetric heat capacities for each material are assumed from the literature (2.42, 1.78, 1.9, and 1.65 MJ m^{-3} K^{-1} for the Al, diamond, SiN_x, and Si, respectively[27–30]). Using this model, we fit for the thermal conductivity of the NCD film. The Al/NCD thermal boundary conductance is also treated as a free parameter and is found to be ~94 MW m^{-2} K^{-1}.

RESULTS AND DISCUSSION

NCD film thickness and columnar structure are shown in the cross-sectional medium angle annular dark field (MAADF) image in Fig. 1(b). From AFM [Fig. 1(c)], the root-mean-square (rms) surface roughness was measured to be 19.6 nm with lateral grain sizes exceeding 300 nm. This is noteworthy considering the diamond film thickness is on the order of 250 nm. Raman measurements [Fig. 1(d)] confirmed the high crystal quality of the diamond film due to the sharp high-intensity sp^3-bonded diamond Raman peak.[31]

Figure 2(a) shows the DC output characteristics of the diamond-capped AlGaN channel HEMT. Despite exposure to 9 hours of H_2 plasma during CVD diamond growth at 500 °C as

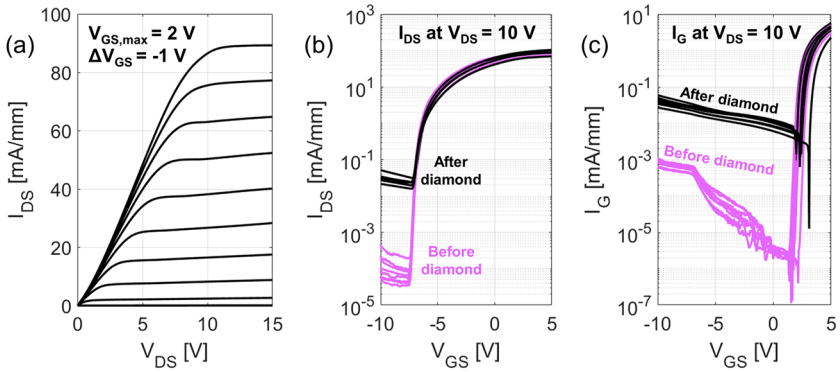

FIG. 2. (a) DC output characteristics of the diamond-capped HEMT. (b) and (c) DC transfer characteristics of the HEMTs before and after diamond growth.

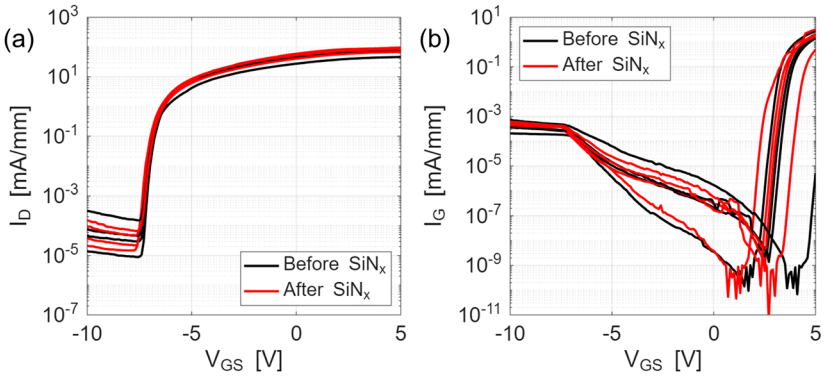

FIG. 3. DC transfer characteristics of (a) drain and (b) gate current of a reference AlGaN channel HEMT before and after deposition of a thin PECVD SiN_x film.

a BEOL process, the HEMTs were still functional, demonstrating gate control and an $I_{DS,max}$ of ≈90 mA/mm. The DC transfer characteristics (I_{DS}–V_{GS} and I_G–V_{GS}) of the HEMTs before and after diamond growth are shown in Figs. 2(b) and 2(c). After diamond growth, off-state leakage significantly increased by about two orders of magnitude, reducing the on/off ratio from 10^6 to 10^4, attributable to an increase in gate leakage current, similar to previous reports.[32,33]

For the origin of the increased leakage current, we first verified that the increase in leakage current was not due to the SiN_x interlayer. Using an uncapped sister sample, we deposited a thin (≈15 nm) PECVD SiN_x film using the same deposition conditions as used when depositing the SiN_x interlayer before diamond growth. As shown in Fig. 3, there was a negligible change in the DC transfer characteristics before and after deposition of the SiN_x film (Fig. 3). There have been reports of Ni/Au contact degradation at high temperatures in HEMTs. Ni/Au mixing and Ni migration have been reported for GaN channel HEMTs operated up to 500 °C in vacuum,[34,35] while gate metal reordering has been reported for $Al_xGa_{1-x}N$ (x = 0.7) channel HEMTs operated at 500 °C in air.[36] EDS was used to assess the elemental composition of the gate electrode of both a reference (uncapped) and a diamond-capped HEMT.

In Figs. 4(a)–4(c), there is a clear distinction between the Ni and Au films in the Schottky gate of the reference HEMT. On the other hand, after NCD growth, the Ni and Au have intermixed, and there is no longer any distinct Ni or Au metal layer observed [Figs. 4(d)–4(f)]. This degradation of the Schottky gate and Au at the metal–semiconductor interface could explain the measured increase in gate leakage.[37,38] However, when we attempted to simulate only the thermal environment during diamond growth by annealing AlGaN HEMTs with a thin SiN_x interlayer (vacuum, 500 °C, 6 h), there was no significant or systematic change in the DC transfer characteristics (Fig. 5). We have also annealed a sister sample of AlGaN HEMTs up to 850 °C in N_2 for 1 h, performed similar cross-sectional EDS analysis as that shown in Fig. 4, and again observed Ni/Au intermixing yet negligible changes in the DC characteristics.[39] Other potential sources of leakage could be hydrogen plasma exposure and/or H-incorporation in the SiN_x interlayer, AlGaN barrier layer, and/or Schottky metal–semiconductor interface,[40,41] or a

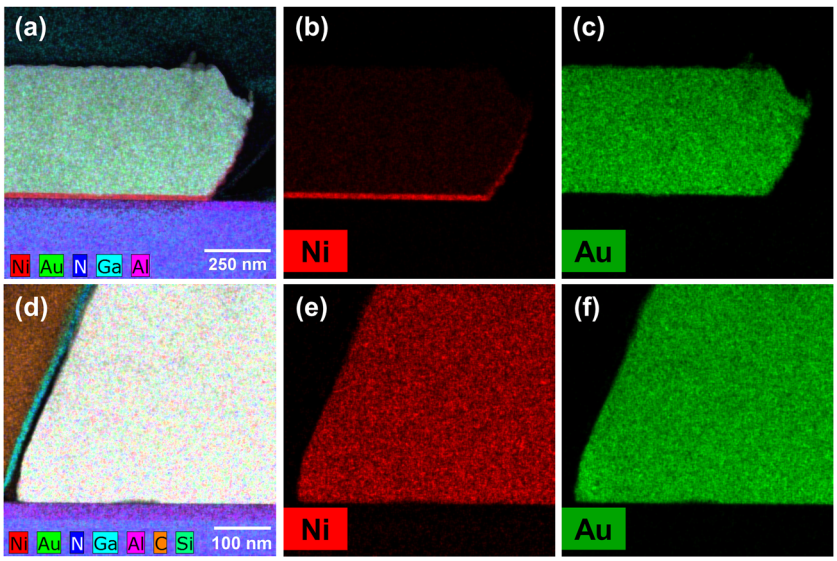

FIG. 4. EDS elemental analysis of the Ni/Au gate electrode of the (a)–(c) uncapped and (d)–(f) diamond-capped HEMTs. (a) and (d) show the elemental analysis with several elements, (b) and (e) show the Ni data, and (c) and (f) show Au data. The slight difference in the appearance of the edge of the gate electrode is due to device processing variability, as the metal lift-off after metal deposition can vary.

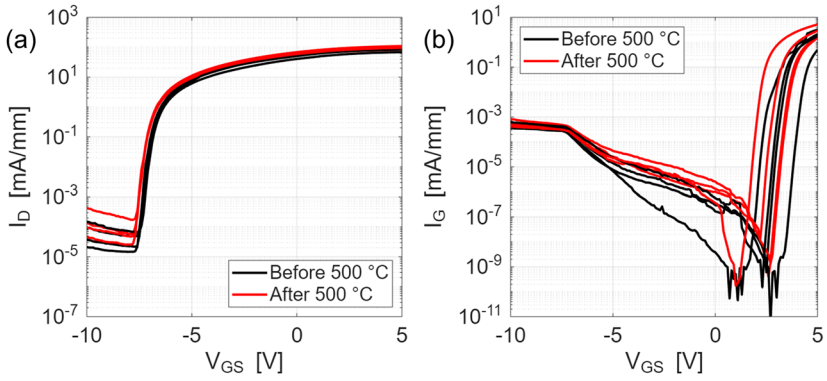

FIG. 5. DC transfer characteristics of (a) drain and (b) gate current of a reference AlGaN channel HEMT capped with a thin PECVD SiN_x film only (no diamond) before and after a 6 h anneal at 500 °C in rough vacuum (≈10 mT).

combination of the thermal and chemical environment during growth, which is the subject of future work.

To quantify the effect of the diamond film on the thermal performance of the device, thermoreflectance imaging was performed on both a reference (uncapped, no diamond) and NCD-capped HEMT under open channel conditions (V_{GS} = 2 V) at steady-state (≈100 ms bias pulse width[22]). Since our thermoreflectance imaging system has a minimum probing wavelength of 365 nm (≈3.4 eV), insufficient for near-bandgap probing of the UWBG AlGaN channel, we applied this method to probe the Au-coated gate electrode, where an average gate temperature rise of the HEMTs was measured. The gate electrode provides a reasonable estimate of the peak temperature rise of the device due to its proximity to the drain-side edge of the gate, where heat generation is highly localized.[23,42,43] Figure 6 shows that the incorporation of the top-side diamond film, acting as a heat spreader, led to a 29% reduction in device-level thermal resistance: 51.8 mm K/W for the reference HEMT down to 36.6 mm K/W for the diamond-capped HEMT.

Subsequently, the cross-plane (along the NCD film growth direction) thermal conductivity of the NCD film on a witness sample was measured using TDTR (see Experimental Methods section)

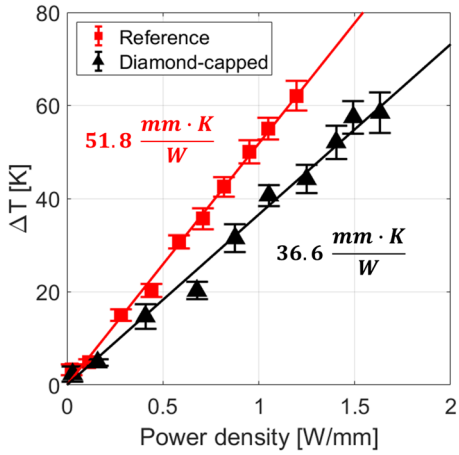

FIG. 6. Average temperature rise of the gate electrode of the uncapped (reference) and diamond-capped HEMTs as a function of power density (V_{GS} = 2 V).

to be 45 ± 25 W m^{-1} K^{-1}. The reported uncertainty accounts for spot-to-spot measurement variability and includes a 5% perturbation in layer thicknesses and thermal conductivities, combined in quadrature. The large uncertainty relative to the measured value can be attributed to low sensitivity to the thermal conductivity of the NCD film as well as a low signal-to-noise ratio at high measurement frequencies. Despite this, the NCD film thermal conductivity is >5× higher than the thermal conductivity of thin Al-rich AlGaN films, which suffer from alloy disorder induced phonon scattering.[9] Moreover, it has been shown that introducing a top-side heat spreading film can also result in electric field spreading.[44–47] This could reduce the electric field concentration at the drain-side edge of the gate and more evenly redistribute the heat generation across the device channel.[48–50] The combination of the NCD thermal conductivity being up to an order of magnitude larger than the AlGaN channel and the potential field spreading, along with the associated coupled electrothermal effects, both explains and contributes to the measured reduction in gate temperature rise of the diamond-capped AlGaN HEMT.

CONCLUSION

In this study, we demonstrated top-side thermal management of high Al-content $Al_xGa_{1-x}N$ (x = 0.68) channel HEMTs via BEOL diamond growth at 500 °C. Thermoreflectance imaging was used to measure the average gate temperature rise and showed a 29% reduction in device-level thermal resistance due to the incorporation of top-side diamond. Using TDTR, the cross-plane thermal conductivity of the NCD film was measured to be 45 ± 25 W m^{-1} K^{-1}, which is expected to be at least >5× higher than the thin AlGaN layers with very low thermal conductivity due to disordered alloy scattering. Regarding electrical performance, the OFF-state leakage of the HEMTs increased following diamond growth. While intermixing of the Ni and Au in the Schottky gate was observed via EDS, we believe another mechanism is responsible for the gate leakage, possibly due to H-plasma exposure and H-incorporation in the SiN_x interlayer, AlGaN barrier, and/or Schottky metal–semiconductor interface. Avenues for future study include (i) investigating electrothermal device performance using novel interlayers,[51] (ii) developing thermally robust gate metallization capable of withstanding BEOL diamond growth, (iii) studying the effect of hydrogen on AlGaN HEMT performance, and (iv) demonstrating diamond growth before gate

metal deposition to allow higher diamond growth temperatures and more readily obtain thicker films and larger lateral grain sizes with higher thermal conductivity.[52,53]

ACKNOWLEDGMENTS

The authors would like to acknowledge Luke Yates (Sandia National Laboratories), Professor Siddharth Rajan (Ohio State University), and Dean Samuel Graham (University of Maryland) for fruitful discussions. The study at the U.S. Naval Research Laboratory was supported by the Office of Naval Research (ONR). Sandia National Laboratories is a multi-mission laboratory managed and operated by National Technology and Engineering Solutions of Sandia, LLC (NTESS), a wholly owned subsidiary of Honeywell International Inc., for the U.S. Department of Energy's National Nuclear Security Administration (DOE/NNSA) under Contract No. DE-NA0003525. This written work is authored by an employee of NTESS. The employee, not NTESS, owns the right, title, and interest in and to the written work and is responsible for its contents. Any subjective views or opinions that might be expressed in the written work do not necessarily represent the views of the U.S. Government. The publisher acknowledges that the U.S. Government retains a non-exclusive, paid-up, irrevocable, worldwide license to publish or reproduce the published form of this written work or allow others to do so for U.S. Government purposes. The DOE will provide public access to results of federally sponsored research in accordance with the DOE Public Access Plan: https://www.energy.gov/downloads/doe-public-access-plan. The study from E.A.S. and P.E.H. was supported as part of APEX (A Center for Power Electronics Materials and Manufacturing Exploration), an Energy Frontier Research Center funded by the U.S. Department of Energy, Office of Science, Basic Energy Sciences under Award No. ERW0345 (thermal property measurements).

AUTHOR DECLARATIONS

Conflict of Interest

The authors have no conflicts to disclose.

Author Contributions

James Spencer Lundh: Conceptualization (equal); Formal analysis (equal); Investigation (equal); Methodology (equal); Validation (equal); Writing – original draft (lead); Writing – review & editing (lead). **Brianna A. Klein**: Conceptualization (equal); Formal analysis (equal); Investigation (equal); Methodology (equal); Validation (equal); Writing – review & editing (equal). **Tatyana I. Feygelson**: Conceptualization (equal); Formal analysis (equal); Investigation (equal). **Daniel J. Pennachio**: Conceptualization (equal); Formal analysis (equal); Investigation (equal). **Andrew A. Allerman**: Conceptualization (equal); Formal analysis (equal); Investigation (equal). **GlenAsia Gonzalez**: Conceptualization (equal); Formal analysis (equal); Investigation (equal). **Emma G. Rocco**: Conceptualization (equal); Formal analysis (equal); Investigation (equal). **Hannah N. Masten**: Conceptualization (equal); Formal analysis (equal); Investigation (equal). **Geoffrey M. Foster**: Conceptualization (equal); Formal analysis (equal); Investigation (equal). **Katie R. Gann**: Conceptualization (equal); Formal analysis (equal); Investigation (equal). **Alan G. Jacobs**: Conceptualization (equal); Formal analysis (equal); Investigation (equal). **Andrew M. Armstrong**: Conceptualization (equal); Funding acquisition (equal); Project administration (equal); Resources (equal); Supervision (equal). **Ethan A. Scott**: Formal analysis (equal); Investigation (equal); Methodology (equal). **Patrick E. Hopkins**: Formal analysis (equal); Investigation (equal); Methodology (equal). **Marko J. Tadjer**: Conceptualization (equal); Formal analysis (equal); Investigation (equal); Resources (equal); Supervision (equal); Writing – review & editing (equal). **Bradford B. Pate**: Conceptualization (equal); Funding acquisition (equal); Project administration (equal); Resources (equal); Supervision (equal). **Karl D. Hobart**: Conceptualization (equal); Funding acquisition (equal); Project administration (equal); Resources (equal); Supervision (equal). **Michael A. Mastro**: Conceptualization (equal); Funding acquisition (equal); Project administration (equal); Resources (equal); Supervision (equal).

DATA AVAILABILITY

The data that support the findings of this study are available within the article.

REFERENCES

[1] J. Y. Tsao, S. Chowdhury, M. A. Hollis, D. Jena, N. M. Johnson, K. A. Jones, R. J. Kaplar, S. Rajan, C. G. Van de Walle, E. Bellotti, C. L. Chua, R. Collazo, M. E. Coltrin, J. A. Cooper, K. R. Evans, S. Graham, T. A. Grotjohn, E. R. Heller, M. Higashiwaki, M. S. Islam, P. W. Juodawlkis, M. A. Khan, A. D. Koehler, J. H. Leach, U. K. Mishra, R. J. Nemanich, R. C. N. Pilawa-Podgurski, J. B. Shealy, Z. Sitar, M. J. Tadjer, A. F. Witulski, M. Wraback, and J. A. Simmons, "Ultrawide-bandgap semiconductors: Research opportunities and challenges," Adv. Electron. Mater. **4**(1), 1600501 (2018).

[2] M. H. Wong, O. Bierwagen, R. J. Kaplar, and H. Umezawa, "Ultrawide-bandgap semiconductors: An overview," J. Mater. Res. **36**(23), 4601–4615 (2021).

[3] T. Nanjo, M. Takeuchi, M. Suita, Y. Abe, T. Oishi, Y. Tokuda, and Y. Aoyagi, "Remarkable breakdown voltage enhancement in AlGaN channel HEMTs," in *2007 IEEE International Electron Devices Meeting* (IEEE, 2007), pp. 397–400.

[4] A. Raman, S. Dasgupta, S. Rajan, J. S. Speck, and U. K. Mishra, "AlGaN channel high electron mobility transistors: Device performance and power-switching figure of merit," Jpn. J. Appl. Phys. **47**(5R), 3359 (2008).

[5] S. Bajaj, F. Akyol, S. Krishnamoorthy, Y. Zhang, and S. Rajan, "AlGaN channel field effect transistors with graded heterostructure ohmic contacts," Appl. Phys. Lett. **109**(13), 133508 (2016).

[6] E. A. Douglas, S. Reza, C. Sanchez, D. Koleske, A. Allerman, B. Klein, A. M. Armstrong, R. J. Kaplar, and A. G. Baca, "Ohmic contacts to Al-rich AlGaN heterostructures," Phys. Status Solidi A **214**(8), 1600842 (2017).

[7] A. G. Baca, A. M. Armstrong, B. A. Klein, A. A. Allerman, E. A. Douglas, and R. J. Kaplar, "Al-rich AlGaN based transistors," J. Vac. Sci. Technol., A **38**(2), 020803 (2020).

[8] *Thermal Management of Gallium Nitride Electronics*, edited by M. J. Tadjer and T. J. Anderson (Elsevier, 2022).

[9] D. Q. Tran, R. D. Carrascon, M. Iwaya, B. Monemar, V. Darakchieva, and P. P. Paskov, "Thermal conductivity of $Al_xGa_{1-x}N$ ($0 \le x \le 1$) epitaxial layers," Phys. Rev. Mater. **6**(10), 104602 (2022).

[10] D. Q. Tran, N. Blumenschein, A. Mock, P. Sukkaew, H. Zhang, J. F. Muth, T. Paskova, P. P. Paskov, and V. Darakchieva, "Thermal conductivity of ultra-wide bandgap thin layers – High Al-content AlGaN and β-Ga_2O_3," Physica B **579**, 411810 (2020).

[11] M. J. Tadjer, T. J. Anderson, K. D. Hobart, T. I. Feygelson, J. D. Caldwell, C. R. Eddy, F. J. Kub, J. E. Butler, B. Pate, and J. Melngailis, "Reduced self-heating in AlGaN/GaN HEMTs using nanocrystalline diamond heat-spreading films," IEEE Electron Device Lett. **33**(1), 23–25 (2012).
[12] B. Klein, A. Allerman, A. Armstrong, M. Rosprim, C. Tyznik, Y. Zhu, C. Joishi, C. Chae, and S. Rajan, "Al-Rich AlGaN transistors with regrown p-AlGaN gate layers and ohmic contacts," Adv. Mater. Interfaces **12**(2), 2301080 (2025).
[13] J. E. Butler and A. V. Sumant, "The CVD of nanodiamond materials," Chem. Vap. Deposition **14**(7–8), 145–160 (2008).
[14] C. Yuan, R. Hanus, and S. Graham, "A review of thermoreflectance techniques for characterizing wide bandgap semiconductors' thermal properties and devices' temperatures," J. Appl. Phys. **132**(22), 220701 (2022).
[15] S. Shin, M. A. Wahab, M. Masuduzzaman, K. Maize, J. Gu, M. Si, A. Shakouri, P. D. Ye, and M. A. Alam, "Direct observation of self-heating in III–V gate-all-around nanowire MOSFETs," IEEE Trans. Electron Devices **62**(11), 3516–3523 (2015).
[16] G. Pavlidis, L. Yates, D. Kendig, C.-F. Lo, H. Marchand, B. Barabadi, and S. Graham, "Thermal performance of GaN/Si HEMTs using near-bandgap thermoreflectance imaging," IEEE Trans. Electron Devices **67**(3), 822–827 (2020).
[17] K. Maize, E. Heller, D. Dorsey, and A. Shakouri, "Fast transient thermoreflectance CCD imaging of pulsed self heating in AlGaN/GaN power transistors," in *2013 IEEE International Reliability Physics Symposium (IRPS)* (IEEE, 2013), pp. CD.2.1–CD.2.3.
[18] S. Martin-Horcajo, J. W. Pomeroy, B. Lambert, H. Jung, H. Blanck, and M. Kuball, "Transient thermoreflectance for gate temperature assessment in pulse operated GaN-based HEMTs," IEEE Electron Device Lett. **37**(9), 1197–1200 (2016).
[19] N. Kumar, D. Vaca, C. Joishi, Z. Xia, S. Rajan, and S. Kumar, "Ultrafast thermoreflectance imaging and electrothermal modeling of β-Ga_2O_3 MESFETs," IEEE Electron Device Lett. **41**(4), 641–644 (2020).
[20] J. H. L. Ling, A. A. O. Tay, K. F. Choo, W. Chen, and D. Kendig, "Measurement of MMIC gate temperature using infrared and thermoreflectance thermography," in *2012 IEEE 14th Electronics Packaging Technology Conference (EPTC)* (IEEE, 2012), pp. 515–518.
[21] J.-H. Bahk and A. Shakouri, "Ultra-fast thermoreflectance imaging for electronic, optoelectronic, and thermal devices," in *2019 IEEE BiCMOS and Compound Semiconductor Integrated Circuits and Technology Symposium (BCICTS)* (IEEE, 2019), pp. 1–7.
[22] J. S. Lundh, Y. Song, B. Chatterjee, A. G. Baca, R. J. Kaplar, A. M. Armstrong, A. A. Allerman, B. A. Klein, D. Kendig, H. Kim, and S. Choi, "Device-level multidimensional thermal dynamics with implications for current and future wide bandgap electronics," J. Electron. Packag. **142**(3), 031113 (2020).
[23] J. S. Lundh, B. Chatterjee, Y. Song, A. G. Baca, R. J. Kaplar, T. E. Beechem, A. A. Allerman, A. M. Armstrong, B. A. Klein, A. Bansal, D. Talreja, A. Pogrebnyakov, E. Heller, V. Gopalan, J. M. Redwing, B. M. Foley, and S. Choi, "Multidimensional thermal analysis of an ultrawide bandgap AlGaN channel high electron mobility transistor," Appl. Phys. Lett. **115**(15), 153503 (2019).
[24] P. Jiang, X. Qian, and R. Yang, "Tutorial: Time-domain thermoreflectance (TDTR) for thermal property characterization of bulk and thin film materials," J. Appl. Phys. **124**(16), 161103 (2018).
[25] D. G. Cahill, "Analysis of heat flow in layered structures for time-domain thermoreflectance," Rev. Sci. Instrum. **75**(12), 5119–5122 (2004).
[26] G. T. Hohensee, W.-P. Hsieh, M. D. Losego, and D. G. Cahill, "Interpreting picosecond acoustics in the case of low interface stiffness," Rev. Sci. Instrum. **83**(11), 114902 (2012).
[27] T. W. Pfeifer, J. A. Tomko, E. Hoglund, E. A. Scott, K. Hattar, K. Huynh, M. Liao, M. Goorsky, and P. E. Hopkins, "Measuring sub-surface spatially varying thermal conductivity of silicon implanted with krypton," J. Appl. Phys. **132**(7), 075112 (2022).
[28] E. A. Scott, K. Hattar, J. L. Braun, C. M. Rost, J. T. Gaskins, T. Bai, Y. Wang, C. Ganski, M. Goorsky, and P. E. Hopkins, "Orders of magnitude reduction in the thermal conductivity of polycrystalline diamond through carbon, nitrogen, and oxygen ion implantation," Carbon **157**, 97–105 (2020).
[29] E. A. Scott, C. Perez, C. Saltonstall, D. P. Adams, V. Carter Hodges, M. Asheghi, K. E. Goodson, P. E. Hopkins, D. Leonhardt, and E. Ziade, "Simultaneous thickness and thermal conductivity measurements of thinned silicon from 100 nm to 17 μm," Appl. Phys. Lett. **118**(20), 202108 (2021).
[30] J. L. Braun, S. W. King, E. R. Hoglund, M. A. Gharacheh, E. A. Scott, A. Giri, J. A. Tomko, J. T. Gaskins, A. Al-kukhun, G. Bhattarai, M. M. Paquette, G. Chollon, B. Willey, G. A. Antonelli, D. W. Gidley, J. Hwang, J. M. Howe, and P. E. Hopkins, "Hydrogen effects on the thermal conductivity of delocalized vibrational modes in amorphous silicon nitride (SiNx:H)," Phys. Rev. Mater. **5**(3), 35604 (2021).
[31] J. Filik, "Raman spectroscopy: A simple, non-destructive way to characterise diamond and diamond-like materials," Spectrosc. Eur. **17**(5), 10–17 (2005).
[32] R. Soman, M. Malakoutian, K. Woo, J.-K. Kim, T. A. Rodriguez, R. P. Martinez, M. DeJarld, M. Tahhan, J. Valliancourt, E. M. Chumbes, J. Laroche, and S. Chowdhury, "Integration of top-side low-temperature diamond on AlGaN/GaN RF HEMT for device-level cooling," Appl. Phys. Lett. **126**(21), 213503 (2025).
[33] J. Yaita, A. Yamada, and J. Kotani, "Growth of microcrystalline diamond films after fabrication of GaN high-electron-mobility transistors for effective heat dissipation," Jpn. J. Appl. Phys. **60**(7), 076502 (2021).
[34] A. E. Islam, N. P. Sepelak, A. T. Miesle, H. Lee, M. Snure, S. Nikodemski, D. E. Walker, N. C. Miller, M. Grupen, K. D. Leedy, K. J. Liddy, A. Crespo, G. R. Hughes, W. Zhu, B. Poling, S. Tetlak, K. D. Chabak, and A. J. Green, "Effect of high temperature on the performance of AlGaN/GaN T-gate high-electron mobility transistors with ~140-nm gate length," IEEE Trans. Electron Devices **71**(3), 1805–1811 (2024).
[35] B. K. Sarker, N. P. Sepelak, K. Nishimura, D. E. Walker, Jr., G. Hughes, I. Wildeson, P. Srivastava, B. Zivasatienraj, K. K. Chu, S. S. Ahmed, K. D. Chabak, A. J. Green, and A. E. Islam, "Temperature dependent characterization of 140–180 nm AlGaN/GaN HEMTs using DC and small-signal RF measurements," Appl. Phys. Lett. **127**(8), 082103 (2025).
[36] P. H. Carey, S. J. Pearton, F. Ren, A. G. Baca, B. A. Klein, A. A. Allerman, A. M. Armstrong, E. A. Douglas, R. J. Kaplar, and P. G. Kotula, "Operation up to 500 °C of $Al_{0.85}Ga_{0.15}N/Al_{0.7}Ga_{0.3}N$ high electron mobility transistors," IEEE J. Electron Devices Soc. **7**, 444–452 (2019).
[37] H. Jung, R. Behtash, J. R. Thorpe, K. Riepe, F. Bourgeois, H. Blanck, A. Chuvilin, and U. Kaiser, "Reliability behavior of GaN HEMTs related to Au diffusion at the Schottky interface," Phys. Status Solidi C **6**(S2), S976–S979 (2009).
[38] D. Marcon, X. Kang, J. Viaene, M. Van Hove, P. Srivastava, S. Decoutere, R. Mertens, and G. Borghs, "GaN-based HEMTs tested under high temperature storage test," Microelectron. Reliab. **51**(9–11), 1717–1720 (2011).
[39] J. S. Lundh, B. A. Klein, A. A. Allerman, A. J. Cantrell, A. Zhao, D. J. Pennachio, G. Gonzalez, E. Cruz, T. M. Nelson, G. M. Foster, A. G. Jacobs, A. D. Koehler, M. J. Tadjer, G. Esteves, T. Olsson, A. M. Armstrong, K. D. Hobart, and M. A. Mastro, "Operation of AlGaN channel HEMTs at 850 C with ON/OFF ratio >10^4," in *IEEE Electron Device Letters Under Review* (IEEE, 2025).
[40] O. Babchenko, J. Dzuba, T. Lalinský, M. Vojs, A. Vincze, T. Ižák, and G. Vanko, "Stability of AlGaN/GaN heterostructures after hydrogen plasma treatment," Appl. Surf. Sci. **395**, 92–97 (2017).
[41] C. Liu, H. Liu, Y. Chen, Z. Cai, Z. He, and P. Lai, "Effect of hydrogen on electrical characteristics of AlGaN/GaN HEMTs after HTO stress," IEEE Trans. Electron Devices **71**(10), 5895–5900 (2024).
[42] E. Heller, S. Choi, D. Dorsey, R. Vetury, and S. Graham, "Electrical and structural dependence of operating temperature of AlGaN/GaN HEMTs," Microelectron. Reliab. **53**(6), 872–877 (2013).
[43] B. Chatterjee, C. Dundar, T. E. Beechem, E. Heller, D. Kendig, H. Kim, N. Donmezer, and S. Choi, "Nanoscale electro-thermal interactions in AlGaN/GaN high electron mobility transistors," J. Appl. Phys. **127**(4), 044502 (2020).
[44] H. N. Masten, J. S. Lundh, T. I. Feygelson, K. Sasaki, Z. Cheng, J. A. Spencer, P.-Y. Liao, J. K. Hite, D. J. Pennachio, A. G. Jacobs, M. A. Mastro, B. N. Feigelson, A. Kuramata, P. Ye, S. Graham, B. B. Pate, K. D. Hobart, T. J. Anderson, and M. J. Tadjer, "Reduced temperature in lateral $(Al_xGa_{1-x})_2O_3/Ga_2O_3$ heterojunction field effect transistor capped with nanocrystalline diamond," Appl. Phys. Lett. **124**(15), 153502 (2024).
[45] B. Prasannanjaneyulu and S. Karmalkar, "Relative effectiveness of high-k passivation and gate-connected field plate techniques in enhancing GaN HEMT breakdown," Microelectron. Reliab. **110**, 113698 (2020).

[46]J. S. Lundh, C. Cress, A. G. Jacobs, Z. Cheng, H. N. Masten, J. A. Spencer, K. Sasaki, J. Gallagher, A. D. Koehler, K. Konishi, S. Graham, A. Kuramata, T. J. Anderson, M. J. Tadjer, K. D. Hobart, and M. A. Mastro, "Electrothermal enhancement of β-$(Al_xGa_{1-x})_2O_3/Ga_2O_3$ heterostructure field-effect transistors via back-end-of-line sputter-deposited AlN layer," J. Appl. Phys. **136**(22), 224502 (2024).
[47]H. Hanawa, H. Onodera, A. Nakajima, and K. Horio, "Numerical analysis of breakdown voltage enhancement in AlGaN/GaN HEMTs with a high-*k* passivation layer," IEEE Trans. Electron Devices **61**(3), 769–775 (2014).
[48]E. Pop and K. E. Goodson, "Thermal phenomena in nanoscale transistors," J. Electron. Packag. **128**(2), 102–108 (2006).
[49]S. Choi, E. R. Heller, D. Dorsey, R. Vetury, and S. Graham, "The impact of bias conditions on self-heating in AlGaN/GaN HEMTs," IEEE Trans. Electron Devices **60**(1), 159–162 (2013).
[50]V. Šodan, H. Oprins, S. Stoffels, M. Baelmans, and I. De Wolf, "Influence of field-plate configuration on power dissipation and temperature profiles in AlGaN/GaN on silicon HEMTs," IEEE Trans. Electron Devices **62**(8), 2416–2422 (2015).
[51]H. T. Aller, T. W. Pfeifer, A. Mamun, K. Huynh, M. Tadjer, T. Feygelson, K. Hobart, T. Anderson, B. Pate, A. Jacobs, J. S. Lundh, M. Goorsky, A. Khan, P. Hopkins, and S. Graham, "Low thermal resistance of Diamond-AlGaN interfaces achieved using carbide interlayers," Adv. Mater. Interfaces **12**(3), 2400575 (2025).
[52]M. A. Angadi, T. Watanabe, A. Bodapati, X. Xiao, O. Auciello, J. A. Carlisle, J. A. Eastman, P. Keblinski, P. K. Schelling, and S. R. Phillpot, "Thermal transport and grain boundary conductance in ultrananocrystalline diamond thin films," J. Appl. Phys. **99**(11), 114301 (2006).
[53]J. Anaya, S. Rossi, M. Alomari, E. Kohn, L. Tóth, B. Pécz, K. D. Hobart, T. J. Anderson, T. I. Feygelson, B. B. Pate, and M. Kuball, "Control of the in-plane thermal conductivity of ultra-thin nanocrystalline diamond films through the grain and grain boundary properties," Acta Mater. **103**, 141–152 (2016).